Assessment of the performance of a turbulence closure model: along the tidally-influenced Kaipara River to the estuary, NZ

Berengere S. Dejeans[1], Julia C. Mullarney[2], Iain T. MacDonald[3] and Glen M. Reeve[3]
[1] University of Waikato, Hamilton, New Zealand; bsfd1@students.waikato.ac.nz
[2] University of Waikato, Hamilton, New Zealand
[3] National Institute of Water & Atmospheric research (NIWA), Hamilton, New Zealand

Abstract
The success of many coastal management projects hinges on the ability to predict the dispersal and settling of sediment particles. Hydrodynamic models have enabled the efficient simulation of sediment transport scenarios at large spatial scales and long time scales. However, these models have limited predictive capacity owing to an incomplete understanding of the processes involved. Turbulence has been shown to have a substantial influence on sediment transport by influencing flocculation (i.e. aggregation of particles), hence driving the behaviour of particles (e.g. deposition, erosion, mixing). Turbulence tends to promote aggregation at low shear stresses and cause floc breakups at high shear stresses. However, despite the key role of turbulence in coastal modelling, there is not a unique approach but several methods to describe turbulence, each based on a different combination of assumptions.
We present modelling results exploring the performance of one closure scheme implemented in a hydrodynamic and sediment transport model, Delft3D. The assessment of the performance of the model is based on comparisons with measured data collected in the heavily sediment-laden Kaipara river, New Zealand. Data was collected in October 2013 using Lagrangian "flocdrifter" platforms released at multiple locations to capture both hydrodynamic and sediment data. In general the model was found to be able to reproduce the right order of magnitude of dissipation rates. However, turbulence characteristics in some sections of the river, usually in the vicinity of abrupt bends, are relatively poorly reproduced. Future work will aim to use the present model to improve the conceptual understanding of fundamental physical processes, in particular the effect of turbulence on flocculation, and floc formation and breakup in estuarine and riverine systems.

Keywords: turbulence, energy dissipation, modelling, closure scheme, Delft3D.

1. Introduction

Flocculation (aggregation of particles) plays a key role in sediment transport within aquatic environments by affecting the size and settling velocity of particles over time. However, the formation and breakup of flocs remain poorly understood. Previous studies have shown that flocculation is largely influenced by turbulence. More precisely, low shear stresses promote the aggregation of particles whereas higher shear stresses cause flocs to break (e.g. [4] [11] [5] [12]). Therefore, in order to accurately model sediment movement, it is necessary to represent the sub-grid scale turbulent processes. Various empirical and statistical approaches have been implemented to model turbulence (e.g. [1]). Most strategies aim to solve the Navier-Stokes equations, which govern fluid flow. One characteristic shared by turbulent flows is their randomness, which makes statistical methods particularly convenient. However, this approach generates more unknown variables than equations, which is known as "the closure problem of turbulence". In order to solve the equations, it is therefore necessary to employ assumptions and approximations (e.g. [9] [1]).
The present paper focuses on the prediction of turbulence using a three-dimensional numerical model to solve the Reynolds-averaged Navier Stokes equations (RANS). We assess the model performance by comparing predictions of a key turbulence parameter with observations collected in a tidally-driven river. The present paper focuses on the performance of one of the closure schemes, namely k-ε, implemented in the software and aims to evaluate how closely the model reproduces the observed distribution of turbulent energy dissipation ε.

2. Study area & Data collection

2.1 Study site
Data were collected in the Kaipara River, located at the Southern end of the Kaipara Harbour, in the North Island of New Zealand (Figure 1). The river frequently meanders, displaying large bends with numerous changes in direction and is characterized by a high sediment load [7].

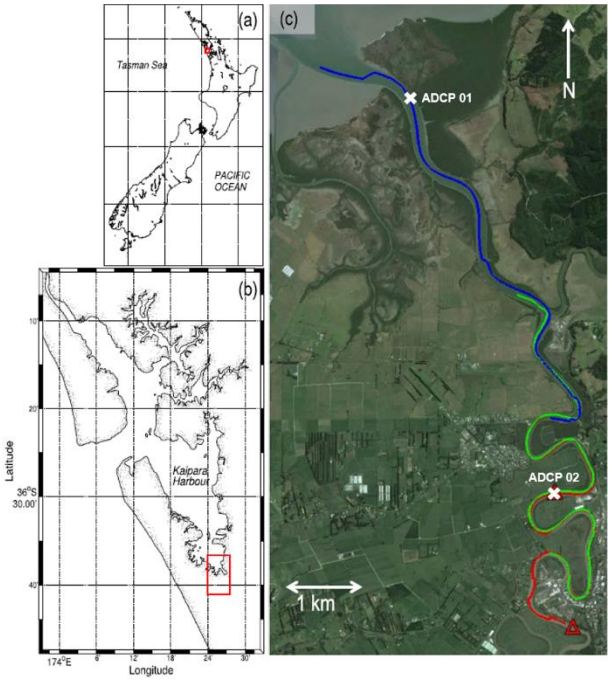

Figure 1 Location of the Kaipara River (a) in New Zealand, (b) in the Kaipara Harbour and (c) tracks of the 3 drifters (different colours) from a single day on Google Earth Images. The white crosses show the Eulerian platforms [7].

2.2 Data collection and analysis

A three-day fieldwork campaign was conducted early October 2013 in the Kaipara River using five Lagrangian platforms ("FlocDrifters"). A drifter system is composed of a floc camera ("FlocCam"), a pulse coherent Acoustic Doppler Current Profiler (ADCP), an Acoustic Doppler Velocimeter (ADV), a Conductivity-Temperature-Depth (CDT) probe) and an Optical Backscatter Sensor (OBS). Several deployments were carried out over three days: three FlocDrifters were released in Lagrangian mode at three different locations, shortly after high tide (Figure 1c; [7]). The FlocDrifters enabled the determination of the Particle Size Distribution (PSD) of the sediment, velocities, the dissipation rate of turbulent kinetic energy ε, Suspended Sediment Concentrations (SSC) and salinity along the river. Table 1 gives a summary of the instrumentation and post-processing. More details are presented in [7]. The calculated dissipation rate of turbulent kinetic energy, ε, exhibited substantial variability along the length of the river, with values between 3.2×10^{-6} and 4.5×10^{-4} m^2s^{-3}.

Table 1 Data collection and processing (after [7]).

Instrument	Measured variable(s)	Derived variable
FlocCam	In situ floc images	Particle size distribution
ADV	3D velocity components (single point)	
ADCP	3D velocity components (profiles)	ε
Turbidity sensor (OBS)	Optical backscatter	SSC
SBE-37 Micro-CAT	Conductivity and temperature	Salinity

Two FlocDrifters were also positioned at two fixed locations (Eulerian mode, Figure 1c) to provide time series of water levels and velocities: 'ADCP 01' corresponds to ADCP near the river mouth and 'ADCP 02' to the upstream ADCP deployment. Quantities were averaged over 5 minutes and then depth-averaged.

3. Model – Set up & Calibration

A hydrodynamic model was developed using with the Delft3D software. Delft3D solves the RANS equations for an incompressible fluid using the shallow water and Boussinesq assumptions [3].
The model was first calibrated in 2DH (depth averaged) mode using water levels and depth-averaged velocities from the fixed ADCPS. A simulation was then run in 3D mode to examine the performance of one of the implemented closure schemes.

3.1 Model set up (2DH)

The computational grid covered about 7 km in length of the lower Kaipara River with rectangular grid cell sizes of approximately 15 x 3 m. The grid starts at the mouth of the Kaipara River, which has been artificially extended a few meters within the estuary basin (Figure 2), and ends further upstream. Bathymetry was interpolated from LiDAR data (provided by the Auckland Council) and a single-beam survey (NIWA).
The model was run for six days: three days of 'spin up' followed by three days for comparison with the field measurements. A time series of water levels is used to force the model at an open boundary located downstream of the river. The forcing time series was derived from observations from the Pouto Point tide gauge located near the mouth of the Kaipara Harbour. Discharge rates, provided by Auckland Regional Council, have also been specified at the upstream boundary of the river.

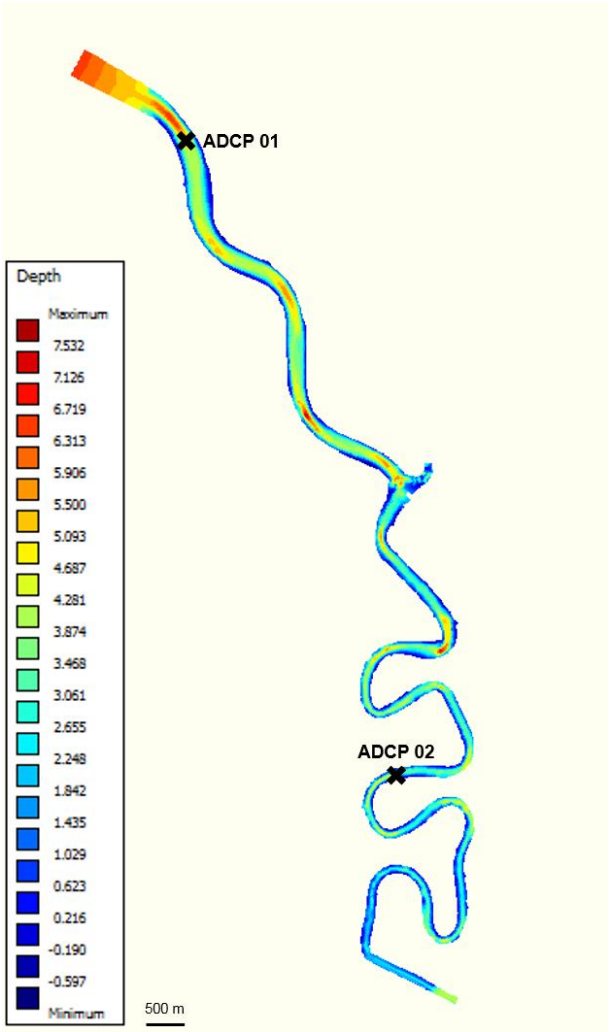

Figure 2 Bathymetry used in the model. The black crosses are the locations of the two fixed ADCPs deployed.

3.2 Model calibration

The model was calibrated by comparing the observed water levels and depth-averaged velocities with the model predictions.

Both the horizontal eddy viscosity and diffusivity were set at 1 $m^2.s^{-1}$. The best calibration was obtained using the Manning formulation for the bottom roughness with a Manning coefficient of 0.02 $m^{1/3}.s^{-1}$. The water levels are well reproduced by the model (Figures 3a and 4a). However, the depth-averaged velocities are globally under-predicted (Figures 3b and 4b). The best calibration in terms of depth-averaged velocities occurs at the observation point located close to the mouth of the river (Figure 3b). Further upstream, the depth-averaged velocities are reasonably well reproduced during flooding events but are poorly predicted during ebbing times (Figure 4b) which might be a result of the discharge boundary. Indeed the time series of discharge used to force the model upstream comes from further upstream of the river whereas the end of the grid is still a tidal area. Additionally, some differences between observations and predictions are likely to be due to the bathymetry. The coverage of the LiDAR and survey data is relatively sparse and may have resulted in errors in interpolation.

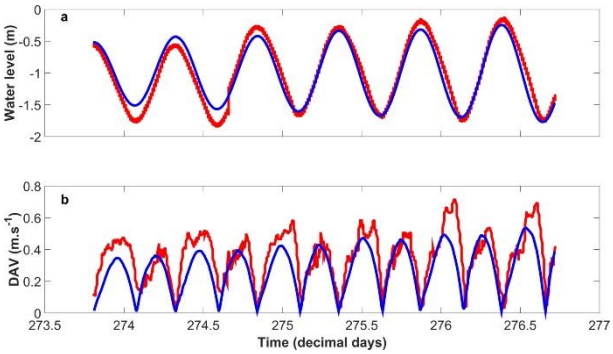

Figure 3 Observed (red lines) and predicted (blue lines) a) water levels and b) depth averaged velocities at the observation point 01 (close to the river mouth).

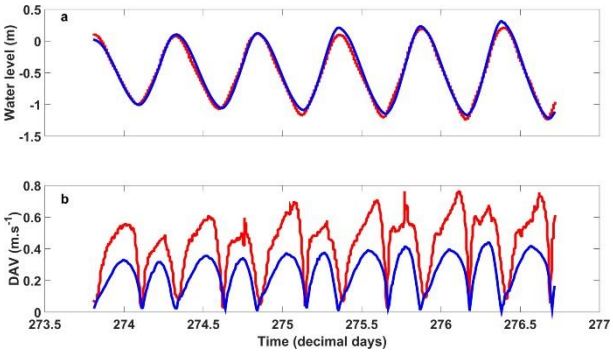

Figure 4 Observed (red lines) and predicted (blue lines) a) water levels and b) depth averaged velocities at the observation point 02 (further upstream in the river).

3.3 3D simulations

A 3D model was created with the same grid, bathymetry, initial and boundary conditions as the calibrated 2D model (Section 3.1 and 3.2) but the domain was split into 10 sigma layers in the vertical. The horizontal eddy viscosity and diffusivity were set to 1 $m^2.s^{-1}$, and the background vertical viscosity and diffusivity were set to the default values 1.0 x 10^{-6} $m^2.s^{-1}$. In 3D simulations, Delft3D computes the vertical turbulent eddy viscosity coefficient ν_V, the vertical turbulent eddy diffusivity coefficient D_V, and the mixing length L (values above background) using (Equations 3.1 and 3.2):

$$\nu_V = c'_\mu \, L \sqrt{k}, \qquad (3.1)$$

$$D_V = \frac{\nu_V}{\sigma_c}, \qquad (3.2)$$

where c'_μ is a constant, k the turbulent kinetic energy and σ_c is the Prandlt-Schmidt number. Delft3D enables the choice of four different approaches to obtain ν_V, D_V and L called closure

schemes: constant (where ν_V, and D_V remain to the background values), algebraic eddy viscosity closure model (AEM), *k-L* and *k-ε*. The fundamental difference between the last three closure schemes is the computation method with which *k*, the dissipation rate of *k* (ε) and/or *L* are calculated. The AEM combines two zero order closure schemes. The *k-L* turbulence closure model analytically defines the mixing length *L* and uses a transport equation for the turbulent kinetic energy *k*, which includes terms for energy dissipation, buoyancy and production (assumed to be dominant; [3]). The present paper focuses on the *k-ε* closure model in which transport equations are solved for both *k* and ε (Equations 3.3 and 3.4):

$$\frac{\partial k}{\partial t} + u\frac{\partial k}{\partial x} + v\frac{\partial k}{\partial y} + \frac{\omega}{d+\zeta}\frac{\partial k}{\partial \sigma} = + \\ + \frac{1}{(d+\zeta)^2}\frac{\partial}{\partial \sigma}\left(D_k\frac{\partial k}{\partial \sigma}\right) + P_k + B_k - \varepsilon, \qquad (3.3)$$

$$\frac{\partial \varepsilon}{\partial t} + u\frac{\partial \varepsilon}{\partial y} + v\frac{\partial \varepsilon}{\partial y} + \frac{\omega}{d+\zeta}\frac{\partial \varepsilon}{\partial \sigma} = + \\ + \frac{1}{(d+\zeta)^2}\frac{\partial}{\partial \sigma}\left(D_\varepsilon\frac{\partial \varepsilon}{\partial \sigma}\right) + P_\varepsilon + B_\varepsilon - c_{2\varepsilon}\frac{\varepsilon^2}{k}, \qquad (3.4)$$

where the eddy diffusivities $D_k = \frac{\nu_{mol}}{\sigma_{mol}} + \frac{\nu_{3D}}{\sigma_k}$ and $D_\varepsilon = \frac{\nu_{3D}}{\sigma_\varepsilon}$, ζ is the water level above the horizontal plane of reference, σ is the scaled vertical coordinate, P_k and P_ε are the production terms, B_k and B_ε are the buoyancy flux terms and $c_{2\varepsilon} = 1.92$.

The terms *k* and ε are then used to compute the mixing length (Equation 3.5):

$$L = c_D\frac{k\sqrt{k}}{\varepsilon}, \qquad (3.5)$$

where $c_D \approx 0.1925$.

3.4 Data processing

As noted above, observations of dissipation rates were collected in a Lagrangian frame of reference. However, Delft3D provides Eulerian output (time series). Therefore, a MATLAB code was constructed in order to extract the predicted values of ε at the time steps and at the grid cells closest to the track observations along the track from the FlocDrifters.

4. Results and discussion

Figures 5 and 6 display the distribution of dissipation rates observed along the river (Lagrangian observations; red dots on Figure 6) and the corresponding values predicted by the model (blue dots). Observed dissipation rates range between 3.2 x 10^{-6} and 4.5 x 10^{-4} m^2s^{-3}. Globally predictions of ε appear to be in the same order of magnitude as the observations, most of them varying between 4.0 x 10^{-6} and 7.9 x 10^{-4} $m^2.s^{-3}$ (light blue rectangle on Figure 6a). Nevertheless, the model tends to significantly under predict dissipation close to the upstream (river input) and downstream (near the mouth) model boundaries, which might be due to boundary conditions and lack of bathymetry data at those locations. Regarding the rest of the river (leaving the extremities aside), the range of predictions appears to be generally in accordance with observations. Yet, even though, the predicted dissipation is slightly higher than the observation at some locations (e.g. at a distance of about 10100 m), the model tends to under-predict the observations. Significant discrepancies (the maximum difference being 5.9 x 10^{-4} $m^2.s^{-3}$) between the observed data and the model results are also observed around some of the bends, where the river abruptly changes direction (i.e. where relatively intense meandering occurs; Figure 6a and b, e.g. green rectangle). Significant over-predictions and under-predictions seem however to remain local and the values of ε are globally under-predicted by the *k-ε* closure scheme.

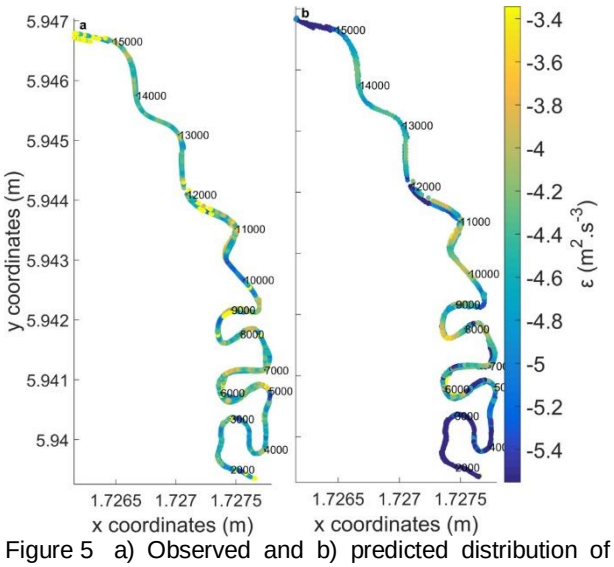

Figure 5 a) Observed and b) predicted distribution of energy dissipation rates along the river. The numbers along the river are the along-river distances from a reference point located upstream of the river.

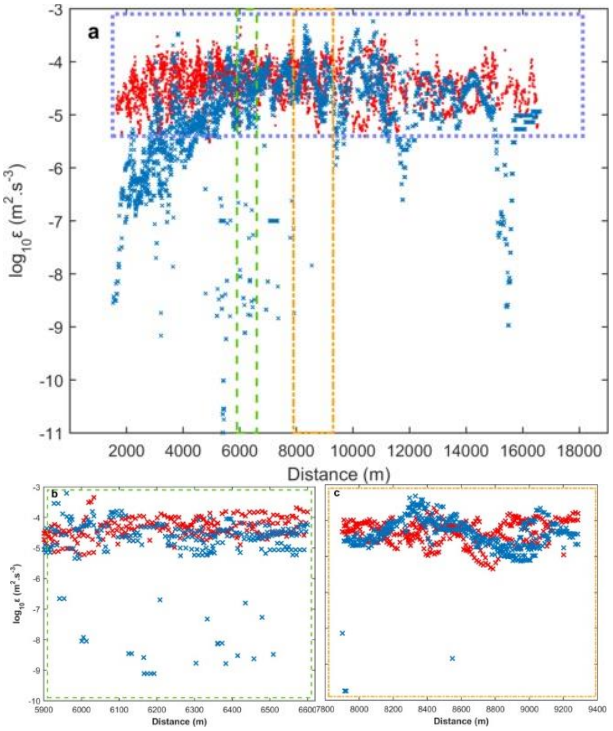

Figure 6 Observed (red) and predicted (blue) dissipation rates of turbulent kinetic energy along the drifter tracks. The light blue rectangle contains most of the predicted ε values. The green and orange boxes indicate examples of locations where the model performs relatively poorly and relatively well in terms of dissipation, respectively. Those short sections are emphasized in b) and c).

The model also enables the output of vertical profiles of the calculated quantities. Figure 7 shows an example of the vertical distribution of ε at the location of the two fixed ADCPs towards the end of an ebb event (continuous lines) and towards the end of a flood event (dashed lines). Profiles of ε are globally close to a logarithmic shape, reaching a minimum at the surface and increasing with depth, regardless of the tidal stage or the locations. The distribution appears to be locally less smooth near the surface at certain time steps around the beginning of floods (e.g. Figure 7b, continuous light blue line). Both at the beginning of ebb and the beginning of flood tide, dissipation rates appear to be slightly higher close to the mouth (corresponding to ADCP 01) than further upstream (ADCP 02; Figure 7, continuous lines). ε remains higher as the water level decreases (Figure 7a); however, closer to the bed, the dissipation increases to similar values at both locations. During the flood tide, however, the predicted trend changes and ε in the middle and upper parts of the water column becomes slightly larger upstream than close to the mouth (Figure 7b). Figure 8 shows the profiles of turbulent kinetic energy (at the same locations and the same time step as ε in Figure 7). *k* is minimum at the water surface and increases with depth at both locations. The turbulent energy is also slightly smaller upstream of the river than near the mouth during ebb and at the beginning of flood in the inferior part of the water column. However, as the water level increases, the kinetic energy becomes higher futher usptream and smaller near the mouth of the river (Figure 7b).

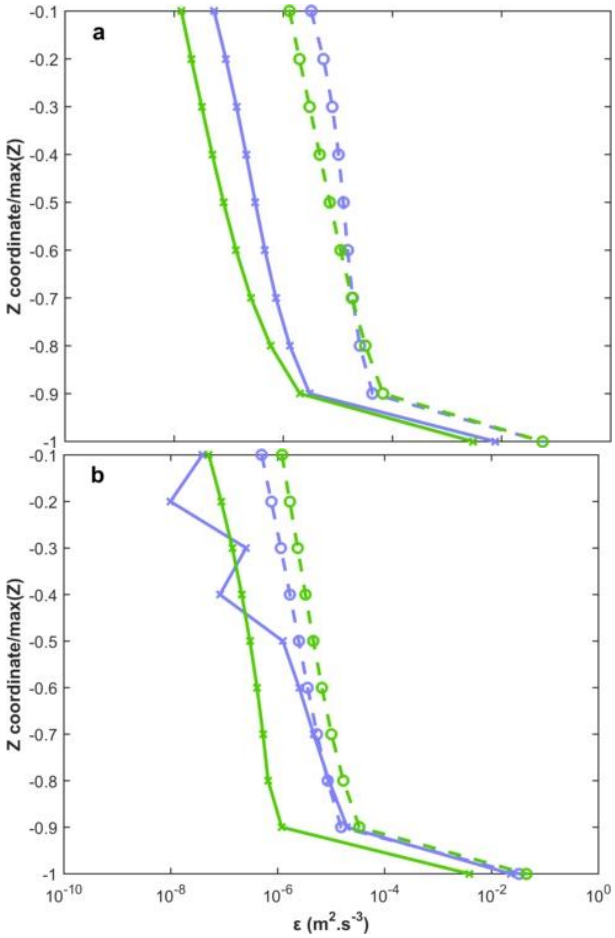

Figure 7 Examples of vertical profiles of modelled ε near the mouth (light blue lines) and further upstream (green lines) at the beginning (continuous lines) and at the end (dashed lines) of (a) an ebb and (b) a flood events.

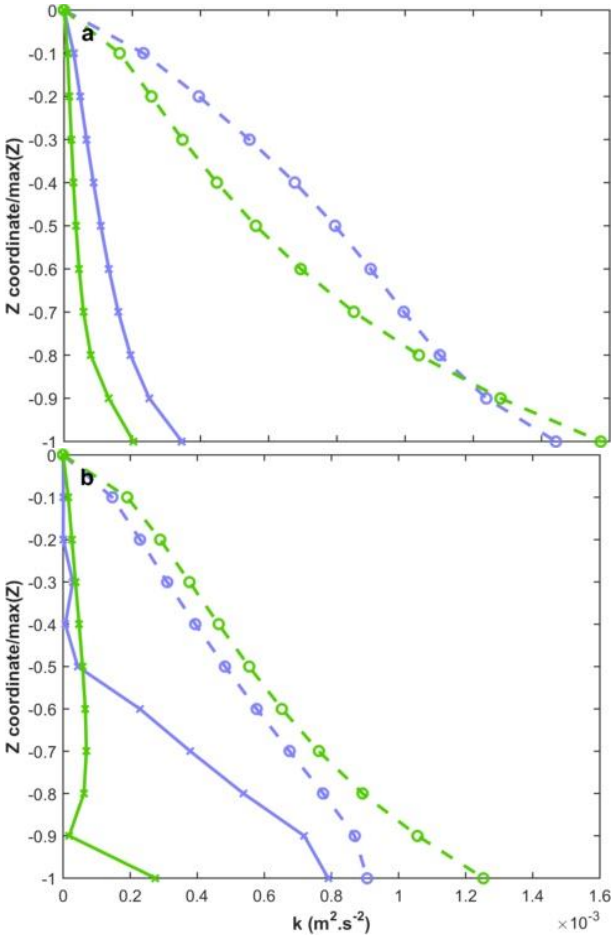

Figure 8 Examples of vertical profiles of modelled k near the mouth (blue) and further upstream (green) at the beginning (continuous lines) and at the end (dashed lines) of (a) an ebbing and (b) a flooding events.

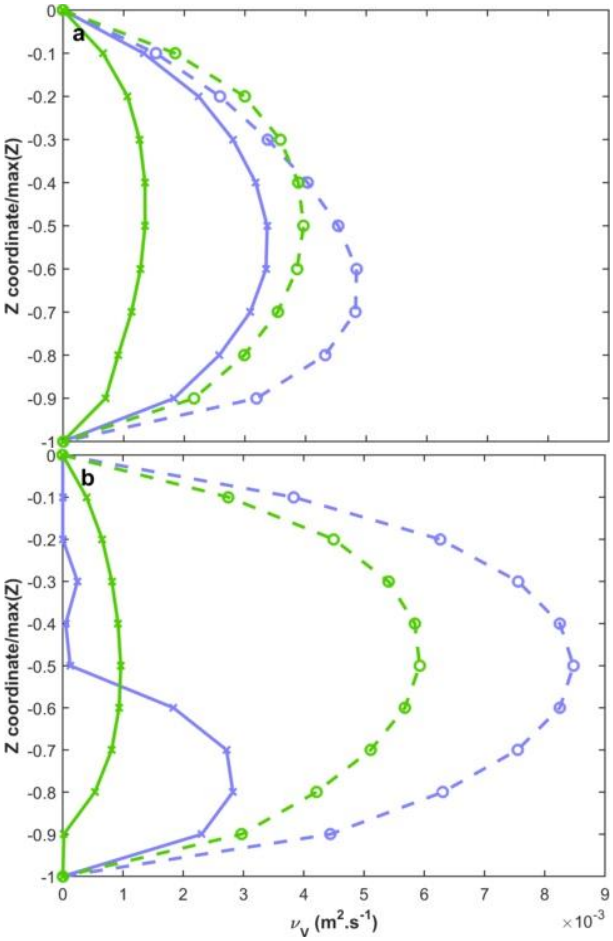

Figure 9 Example of a vertical profile of modelled viscosity near the mouth (light blue lines) and further upstream (green lines) at the beginning (continuous lines) and at the end (dashed lines) of an (a) ebbing and of a (b) flooding events.

Figure 9 illustrates profiles of viscosity predicted by the model at the locations of the fixed ADCP mooring sites. Figure 9a shows the viscosity profile predicted during an ebbing tide and Figure 9b during a flooding tide. The modelled vertical eddy viscosity profiles have a parabolic profile where the maximum viscosity occurs around mid-depth (around 2.8 m and 1.7 m below surface for ADCP01 and ADCP02, respectively). In general, the viscosity is higher at the location of the first ADCP, close to the mouth of the river, regardless of the stage of the tide. In a similar manner to the dissipation and kinetic energy (Figures 7 and 8), the viscosity in the upper part of the water column tends to be small at the beginning of flooding events and displays the parabolic shape in the lower part of the water column (Figure 9b, continuous light blue line). As the water level rises however the viscosity increases more rapidly below the surface and the vertical distribution of viscosity reaches becomes parabolic shape from the sea surface to the seabed (Figure 9b, dashed light blue line). Both during ebb and during flood, viscosity tends to increase over the event.

The *k*-ε turbulence closure model implemented in Delft3D_Flow reproduced the right order of magnitude of energy dissipation rates along the river when comparing to the Lagrangian observations. However, some significant discrepancies can be observed in some sections of the river, which seem to correspond to relatively abrupt changes of direction of the river (i.e. intensive meandering; Figure 6).

[6] found a vertical distribution of ε displaying a maximum near to the water surface, a minimum around the middle of the water column and a second maximum, usually smaller, near the bed. The first maximum has however often been attributed to the effect of wind (e.g. [2]). The general shapes of the vertical distributions of ε, k, and ν obtained with the present model are relatively similar to the ones found in literature (e.g. [10] [8]). The vertical profiles of energy dissipation and turbulent kinetic energy (Figures 7 and 8) indicate that, as the water level decreases, ε and *k* are higher near the mouth of the river than further upstream. However, during flood, the energy dissipation and kinetic energy are globally higher near the mouth when the tide starts

to propagate but, as the water level rises, both increase more significantly upstream than downstream. This faster rate of increase could be caused by the considerable meandering of the river further upstream [8].

5. Summary

A model was developed with the Deltf3D software in order to assess how well it could reproduce turbulence in the tidally-driven Kaipara River. After calibrating the model in 2D, a simulation was run in 3D with the k-ε closure scheme and model predictions were compared to Lagrangian measurements of energy dissipation collected along the river. The model could reproduce the right order of magnitude but significant discrepancies could be observed at some sections of the river. Vertical distributions of dissipation, turbulent kinetic energy and eddy viscosity predicted by the model display shapes similar to ones found in literature.
Future work will first focus on improving the model set up. It could include the collection of more bathymetric data and the calculation of the upstream discharge from water levels. Indeed the lack of data, leading to errors in interpolation, could explain part of the poor predictive skills of the model at some sections of the river. A comparison of the model predictions with the other implemented closure schemes (constant, algebraic and k-L) will be undertaken. The model will then be used to investigate sediment transport in the Kaipara River and in particular to study the effects of turbulence on flocculation.

6. Acknowledgements

This work was funded by the National Institute of Water and Atmospheric research (NIWA). We thank Dr Mark Pritchard for providing data and for their assistance in the development of the Delt3D model as well as the Auckland Regional Council.

7. References

[1] Burchard, H., Craig, P. D., Gemmrich, J. R., van Haren, H., Mathieu, P. P., Meier, H. M., ... & Smyth, W. D. (2008). Observational and numerical modeling methods for quantifying coastal ocean turbulence and mixing. Progress in oceanography, 76(4), 399-442.

[2] Csanady, G. T. (1984). The free surface turbulent shear layer. Journal of physical oceanography, 14(2), 402-411.

[3] Deltares (2014). Delft3D-FLOW - User Manual. Tech. rep. Version Version: 3.15.34158.684 pp.

[4] Dyer, KR (1989). “Sediment processes in estuaries: future research requirements”. In: Journal of Geophysical Research: Oceans 94.C10, pp. 14327–14339.

[5] Dyer, K. R., & Manning, A. J. (1999). Observation of the size, settling velocity and effective density of flocs, and their fractal dimensions. *Journal of sea research*, *41*(1), 87-95.

[6] Feddersen, F., Trowbridge, J. H., & Williams III, A. J. (2007). Vertical structure of dissipation in the nearshore. *Journal of Physical Oceanography*, *37*(7), 1764-1777.

[7] MacDonald, I. T., & Mullarney, J. C. (2015)]. A novel “FlocDrifter” platform for observing flocculation and turbulence processes in a lagrangian frame of reference. Journal of Atmospheric and Oceanic Technology, 32(3), 547-561.

[8] Sukhodolov, A. N. (2012). Structure of turbulent flow in a meander bend of a lowland river. *Water Resources Research*, *48*(1).

[9] Tennekes & Lumley, 1973] Tennekes, H. and J.L. Lumley (1973). A First Course in Turbulence. MIT Press Design Department, p. 300. isbn: 0 262 20019 8.

[10] Warner, J. C., Sherwood, C. R., Arango, H. G., & Signell, R. P. (2005). Performance of four turbulence closure models implemented using a generic length scale method. Ocean Modelling, 8(1), 81-113.

[11] Winterwerp, Johan C. (1998). “A simple model for turbulence induced flocculation of cohesive sediment”. In: Journal of Hydraulic Research 36.3, pp. 309–326.

[12] Winterwerp, J.C. (2002). “On the flocculation and settling velocity of estuarine mud”. In: Continental Shelf Research 22.9, pp. 1339 –1360. issn: 0278-4343.